channels and unchanneled valleys, as well as from channel heads, these plots demonstrate that channel head locations define a threshold transition between channeled and unchanneled regions of the landscape. See (4) for further discussion of field techniques and criteria used to define channel head locations.
24. D. L. Johnson, *Quat. Res. (N.Y.)* 8, 154 (1977); J. D. Sims, Ed., *Geol. Soc. Am. Spec. Pap. 214* (1988); COHMAP members (P. M. Anderson *et al.*), *Science* 241, 1043 (1988); S. Rypins, S. L. Reneau, R. Byrne, D. R. Montgomery, *Quat. Res. (N.Y.)* 32, 72 (1989).
25. We used the model TOPOG [E. M. O'Loughlin, *Water Resour. Res.* 22, 794 (1986)] to create a digital land surface from topography digitized from low-altitude stereo air photographs.
26. W. E. Dietrich, C. J. Wilson, D. R. Montgomery, J. McKean, R. Bauer, in preparation.
27. The lower limit to the range selected to illustrate areas just below the threshold zone in Fig. 5 is arbitrary. The range depicted was selected to illustrate that areas marginally below the channelization threshold range essentially surround areas of convergent topography. These zones expand upslope if a wider range in values is used and contract toward the margins of the channel network if a more restrictive range is adopted. Some of the areas depicted as in the transition zone are steep areas underlain by thin soil profiles or areas of bedrock outcrop in which the processes influencing channel initiation differ from the rest of the soil-mantled drainage basin. In general, however, the transition zones should define those parts of the landscape most sensitive to environmental change, an interpretation supported by a close correspondence with the extent of Holocene valley fills.
28. S. A. Schumm, *Geol. Soc. Am. Bull.* 67, 597 (1956).
29. The coastal Oregon study area consists of 12 second- and third-order basins near Coos Bay, Oregon. The area is covered by a managed forest and underlain by relatively undeformed Tertiary sandstone. The northern California study area is composed of four adjacent second- to fourth-order basins in the Tennessee Valley area north of San Francisco, California. The area is covered by coastal scrub and grassland vegetation and is underlain by highly deformed Mesozoic sandstone, chert, and greenstone of the Franciscan Assemblage. The southern California study area consists of two third-order basins located in the southern Sierra Nevada about 45 km east of Bakersfield, California. The area is covered with an open oak forest and is underlain by Mesozoic granitic rocks. Further descriptions of the study areas, and the channel initiation processes acting within them, are in (4, 5).
30. This research was funded by NSF grants EAR-8451175 and EAR-8917467. We thank J. McKean for digitizing the elevation data for Tennessee Valley; C. J. Wilson and R. Reiss for assistance with TOPOG; and W. Rankin, the Golden Gate National Recreation Area, and the Weyerhaeuser Company for access to our study areas. We also thank J. Kirchner, C. J. Wilson, D. Tarboton, and several reviewers for commenting on drafts of this manuscript.

7 August 1991; accepted 25 November 1991

Electrical Transport Properties of Undoped CVD Diamond Films

L. S. Pan,* D. R. Kania, S. Han, J. W. Ager III, M. Landstrass, O. L. Landen, P. Pianetta

Polycrystalline diamond films synthesized by microwave-assisted chemical vapor deposition (MACVD) were examined with transient photoconductivity, and two fundamental electrical transport properties, the carrier mobility and lifetime, were measured. The highest mobility measured is 50 centimeters squared per volt per second at low initial carrier densities ($<10^{15}$ per cubic centimeter). Electron-hole scattering causes the carrier mobility to decrease at higher carrier densities. Although not measured directly, the carrier lifetime was inferred to be 40 picoseconds. The average drift length of the carriers is smaller than the average grain size and appears to be limited by defects within the grains. The carrier mobility in the MACVD films is higher than values measured in lower quality dc-plasma films but is much smaller than that of single-crystal natural diamond.

With the development of synthetic diamond films made by chemical vapor deposition (CVD), diamond devices have been envisioned for consumer and industrial products such as space applications, process control equipment, electric power installations, and automobiles. Diamond electronic devices would be ideally suited for applications associated with high power, high frequency, high temperatures, and harsh radiation environments. This is clear from the extreme physical and electronic properties of diamond. Single-crystal natural diamond has the highest room-temperature thermal conductivity (20 W cm^{-1} K^{-1}) (1), the lowest coefficient of thermal expansion (0.8×10^{-6}) (2), the highest electron- and hole-saturated velocities (1.5×10^7 cm s^{-1} and 1.05×10^7 cm s^{-1}, respectively) (3), the highest electrical breakdown field (10^7 V cm^{-1}) (4), a low dielectric constant (5.7) (5), high intrinsic resistivity (as high as 10^{20} ohm-cm) (6), and high electron and hole mobilities (~2000 and 1200 cm^2 V^{-1} s^{-1}, respectively). In addition, diamond is chemically inert and radiation-hard. The Keyes (7) and Johnson (8) figures of merit for diamond are nearly two orders of magnitude better than that for silicon. Simple prototype diamond devices, such as *p-n* junction diodes and transistors containing both natural and synthetic diamond, have been fabricated [see (9)].

L. S. Pan and P. Pianetta, Stanford Synchrotron Radiation Laboratory, Stanford Linear Accelerator Center Bin 99, Post Office Box 4349, Stanford, CA 94309.
D. R. Kania, S. Han, O. L. Landen, Lawrence Livermore National Laboratory, L-473, Post Office Box 5508, Livermore, CA 94550.
J. W. Ager III, Center for Advanced Materials, Lawrence Berkeley Laboratory, University of California, Berkeley, CA 94720.
M. Landstrass, Crystallume, 125 Constitution Avenue, Menlo Park, CA 94025.

*To whom correspondence should be addressed at Lawrence Livermore National Laboratory, L-476, Post Office Box 5508, Livermore, CA 94550.

The recent growing interest in diamond stems from significant advances in the growth of synthetic diamond films made by CVD, which have led to films of large area and thickness and of improved quality (10). In the CVD method, a gas mixture containing C and H is excited to form a plasma. A typical gas mixture contains ~1% methane and ~99% H_2. Under certain gas pressure and substrate temperature ranges (typically 20 to 100 torr and 700° to 950°C, respectively), graphitic (sp^2-bonded) C growth is suppressed, while diamond-bonded (sp^3-bonded) C is successfully deposited. Films with little or no nondiamond-bonded C can now be deposited on a variety of substrates.

All CVD films deposited on nondiamond substrates to date are polycrystalline. Even so, the electrical and optical properties of CVD films are approaching those of natural diamond. For example, the resistivity of natural insulating diamond is typically greater than 10^{15} ohm-cm, and values as high as 10^{13} ohm-cm have been achieved in CVD films (11). Being able to produce CVD films with high resistivity is promising, but resistivity alone does not determine whether a material is suitable for electronic applications because the resistivity can depend on carrier concentration, carrier mobility, and space charge (12). Traditional characterization uses the Hall effect to determine both the mobility and the concentration of the carriers, but in undoped, insulating materials this measurement is difficult because of the low intrinsic carrier concentration (13).

A powerful technique that is suitable for characterizing such resistive materials is transient photoconductivity (PC), in which a known carrier concentration is created by intrinsic photoexcitation. From the magnitude of the photocurrent and its transient decay, two fundamental properties for device applications, the mobility and lifetime of the carriers, can be determined. This technique has been applied to natural IIa diamonds (14). In this report we discuss results on CVD polycrystalline diamond

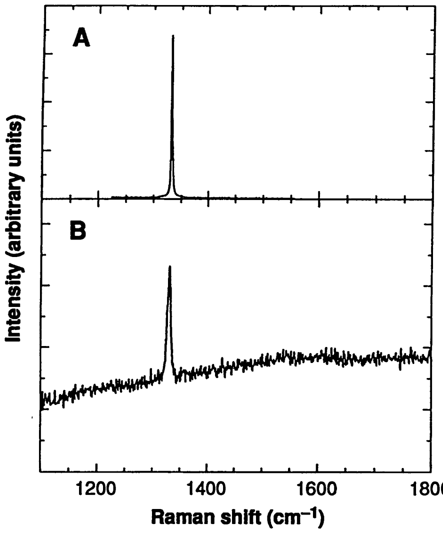

Fig. 1. The Raman spectra of (**A**) a natural type IIa diamond and (**B**) a MACVD-grown diamond film. Both contain a sharp peak at 1332 cm^{-1} and a featureless background, indicative of diamond-bonded C.

films. Most of our results will pertain to films deposited by microwave-assisted CVD (MACVD); we also make some comparisons to earlier dc-plasma CVD films (*15*). Our observations show that the optical absorption, resistivity, and mobility of the films improved with better growth and processing.

Although a variety of excitation sources are being used with CVD to produce diamond, MACVD is one of the most popular because of its ability to deposit high-quality material with low impurity concentrations. The technique is capable of depositing diamond on a variety of substrates. In this study, we deposited the films on two 2-inch silicon substrates (*p*-type, 1 to 10 ohm-cm), prescratched with diamond powder. Films 3 and 6 μm thick were grown, and several samples 1 cm by 1 cm from each wafer were examined. The films were annealed after deposition at 600°C for 1 hour in a nitrogen atmosphere to improve and stabilize electrical resistivity (*11*). The optical absorption coefficients were also measured on these films for light of energy 6.11 eV (the energy of the laser to be described below). For natural diamond the optical absorption coefficient is 5500 cm^{-1} (*16*) at this energy. An integrating sphere was used to measure the absorption coefficients in the films at this photon energy, which were 7,500 (±2,000) cm^{-1} for the 6-μm film and 10,000 (±2,000) cm^{-1} for the 3-μm film. In addition to electrical resistivity and optical absorption, the Raman spectrum of the films was measured.

Raman spectroscopy is one of the most widely used techniques for characterizing diamond films (*17*). The first-order Raman scattering from diamond produces a single sharp line at 1332 cm^{-1}, characteristic of the diamond bonding. The technique is sensitive to the presence of nondiamond bonding, which would lead to a broad background centered around 1550 cm^{-1} (*18*). The spectra of the microwave film samples showed only the sharp Raman peak characteristic of diamond with very little amorphous C, indicative of a high-quality diamond film (Fig. 1). Many of the properties of these films approach those of single-crystal type IIa diamonds. Properties of the dc films studied earlier were much poorer (Table 1).

To prepare the films for PC measurements, we removed the silicon substrate and applied electrical contacts. The diamond film was first epoxied to an alumina substrate, and then the silicon was etched away with a mixture of hydrofluoric and nitric acids. Electrical contacts in the form of a microstrip transmission line 1 mm wide of 200 Å titanium and 5000 Å gold were then evaporated on top of the diamond film and the alumina, leaving a gap of 1 mm in the center of the diamond as the photoactive region. The line served both as the contacts and as the top conductor of the microstrip transmission line. A voltage applied across the 1-mm gap defined the electric field needed for electrical conduction. Nearly linear current-voltage curves were measured, suggestive of good ohmic contacts.

The PC technique uses light to excite free carriers for conduction. Photons with energy greater than the 5.5-eV band gap are desired for intrinsic excitation. We used a frequency-tripled dye laser to provide 6.11-eV photons (*19*). Each laser pulse was 3 to 5 ps in length and contained up to 50 μJ. The laser light was directed onto the 1-mm gap, and the absorbed energy was calculated from the measured incident energy and measured absorption coefficients (Table 1). We approximated the density of initially excited carriers by dividing the absorbed energy in one absorption depth by the energy needed to create one electron-hole pair, that is, the photon energy, and by the volume of energy absorption, which was approximated by the area of the beam times the reciprocal of the absorption coefficient.

Treating the laser excitation as a delta function, we can describe the carrier density $n(t)$ by an exponential decay: $n(t) = n_0 \exp(-t/\tau)$, where n_0 is the initial excitation density and τ is the lifetime of the free carriers. The measured current is proportional to $n(t)$ and the mobility μ. At low excitation densities, the measured decay time is equal to the lifetime of the free carriers. The integrated charge per pulse is proportional to the product $\mu\tau$, and, because τ can be measured from the decay, μ can also be determined. One shortcoming of this technique is its inability to distinguish between electron and hole contributions to the current. The measured current is actually a weighted sum of the two contributions, with the weighting factor being the respective lifetimes: $\mu\tau = \mu_n\tau_n + \mu_p\tau_p$, where μ_n and μ_p and τ_n and τ_p are the electron and hole mobilities and lifetimes, respectively. In most cases, however, the photocurrent can be described by a single carrier density without distinguishing between electron and hole conduction. This approach has worked well in the treatment of natural diamonds (*14*).

Applying this technique to natural IIa diamonds, we measured lifetimes that were sample-dependent, ranging from 100 to 600 ps. Panchhi and van Driel (*20*) reported a lifetime of 150 ps in insulating diamond excited by sub–band-gap light. We also observed a range for the low-density mobility, μ_0, from 500 to 3000 $cm^2\ V^{-1}\ s^{-1}$, again depending on the sample. The temperature dependence of μ_0 suggests that the scattering mechanism is acoustic phonon scattering (*21*). The results from our measurements are in good agreement with earlier studies on single-crystal diamonds based on the use

Table 1. The microwave films have properties approaching those of the IIa diamond; FWHM, full width at half maximum.

Property	dc film (*15*)	Microwave film	Single-crystal IIa diamond
Thickness	≤1 μm	3 and 6 μm	$1 \times 1 \times 3\ mm^3$
Grain size	Hundreds of angstroms to 1 μm	~1 μm	Single crystal
Raman	Broad graphitic background	Peak, 1,332.5 to 1,332.9 cm^{-1} (FWHM, 5.6 to 6.4 cm^{-1}); little graphitic background	1,332.4, peak (FWHM, 2.4 cm^{-1})
Resistivity (ohm-cm)	$\leq 10^4$	10^8 to 10^{12}	$>10^{12}$
Absorption at 6.1 eV (1/cm)	>40,000	6,000 to 10,000	5,500 (*16*)

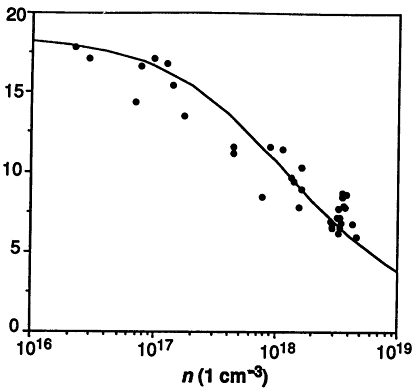

Fig. 2. The $\mu\tau$ product for the 3-μm film. From the calculated fit, $\mu_0 = 43$ cm^2 V^{-1} s^{-1} and $\tau = 44$ ps for the 3-μm film (at an applied field of 3.0 kV cm^{-1}, shown here). For the 6-μm film, $\mu_0 = 50$ cm^2 V^{-1} s^{-1} and $\tau = 28$ ps (at a field of 4.0 kV cm^{-1}).

of a variety of techniques. For example, Redfield (*22*) reported an electron mobility (μ_n) of 1800 cm^2 V^{-1} s^{-1} and a hole mobility (μ_p) of 1200 cm^2 V^{-1} s^{-1} using the Hall effect, Konorova and Shevchencko (*23*) measured μ_n to be 2000 cm^2 V^{-1} s^{-1} and μ_p to be 1500 cm^2 V^{-1} s^{-1} using the Hall effect, and Canali *et al.* (*3*) reported μ_n to be 2400 and μ_p to be 2100 cm^2 V^{-1} s^{-1} using particle excitation and time-of-flight measurements. Exact agreement between studies is not expected because each natural diamond is unique in impurity and defect concentrations.

When the technique was applied to the microwave films, the PC decay was extremely fast at all laser intensities and bias voltages. The material appeared to have a lifetime less than the response time of the system (60 ps). Thus, the measurements could only set an upper limit on the lifetime. From the total integrated charge in the pulse, however, we could still measure the product of the mobility and the lifetime. Following the same procedure used for natural diamonds (*24*), we measured this product as a function of excited carrier density. As was true in the single-crystal IIa diamonds, the $\mu\tau$ product in these films was a decreasing function of excitation density. The decrease was due to increased electron-hole scattering at higher densities. This scattering reduced the effective mobility by altering the total momentum of the electrons and holes. The mobility can be expressed analytically with the relation: $\mu^{-1} = \mu_0^{-1} + \mu_{eh}^{-1}$, where μ_0 is due to scattering mechanisms independent of the density and μ_{eh} is the mobility associated with electron-hole scattering. The following expression describes μ_{eh} in diamond (*24*):

$$\mu_{eh} = 3.11 \times 10^{16} \frac{T^{3/2}}{n} \times \left[\ln\left(1 + 1.77 \times 10^8 \frac{T^2}{n^{2/3}}\right)\right]^{-1} \text{cm}^2\,\text{V}^{-1}\,\text{s}^{-1} \quad (1)$$

where T is the temperature. The points in Fig. 2 show the $\mu\tau$ product extracted for the 3-μm film as a function of carrier density. The solid line in Fig. 2 is calculated from the analytic expression. In matching the $\mu\tau$ product with the calculated curve for the mobility, the proportionality constant was the inferred lifetime. Thus, by using Eq. 1 to describe the mobility at high densities, we could determine the lifetimes, even though they could not be directly measured.

To our knowledge, the only other studies related to these are dc measurements using the Hall effect on *p*-type (*25*) and *n*-type (*26*) doped CVD films by Okano at Tokai University and Nishimura (*27*) at Kobe Steel. Okano arrived at a hole mobility of 44 cm^2 V^{-1} s^{-1} and an electron mobility of 50 cm^2 V^{-1} s^{-1}, whereas we inferred 50 (±10) cm^2 V^{-1} s^{-1} for the combined electron and hole mobility. Nishimura reported a mobility around 1 cm^2 V^{-1} s^{-1}. He attributed this unusually low value to impurity band formation and scattering by ionized and neutral impurities, which was strong as a result of heavy doping concentrations (>10^{19} cm^{-3}).

The quality of the microwave films was much better than that of the earlier dc-plasma CVD films (*15*). The dc-plasma films contained a substantial amorphous C content and may be termed diamond-like C films. The Raman scattered signal from these films at 1330 cm^{-1} showed only a small amount of sp^3 bonding and a significant background from nondiamond-bonded C. The electrical resistivity of the dc-plasma films was also much lower than that of the microwave films (≤10^4 ohm-cm). The absorption coefficient at 6.11 eV was considerably larger, varying from film to film between 4.5 × 10^4 and 6.8 × 10^4 (±5000) cm^{-1}.

The sensitivity to photoexcitation also reflected the lower quality of the dc-plasma films compared to the microwave films. The $\mu\tau$ products for the dc-plasma films were on the order of 10^{-11} to 10^{-12} cm^2 V^{-1}, compared to 10^{-9} cm^2 V^{-1} for the microwave films and 10^{-6} cm^2 V^{-1} for the natural diamonds. An undetermined scattering mechanism dominated even the electron-hole scattering effect at high densities in the dc-plasma films, and thus no density dependence was observed in the $\mu\tau$ product. In most of the dc films, the decay consisted of a fast component similar to that of IIa diamonds but also contained a much longer tail that persisted for as long as 50 ns, most likely due to thermal detrapping from shallow trap states.

With both microwave and dc films, no obvious relation was observed between the decay times and the average grain size, which varied from 0.01 to 2 μm, depending on the sample. A simple estimate of the distance traveled before capture indicates that most of the carriers do not drift far enough to reach the grain boundaries (Table 2). This distance can be described by the average drift distance d, given by $d = \mu E \tau$, where E is the applied field. The estimated drift mobilities (Table 2) are much lower than values measured in natural diamonds and are most likely limited by scattering and capture by defects within the crystallites. The drift distance at the highest applied fields (Table 2) and the ratio of d to the average grain size g in the films are much larger for the microwave films than for the dc films, a reflection of the improved mobility. The ratio in general was much less than

Table 2. Conditions and results for the microwave and dc-plasma films. The error in the decay times for the fast component is about 30%. The error in the mobilities is a factor of 2. The drift distance d is compared to the average grain size g in the various samples; the ratio suggests that most carriers do not traverse a typical grain.

Sample	Maximum field (V cm^{-1})	Fast decay (ps)	Slow decay (ns)	Resistivity (ohm-cm)	μ (cm^2 V^{-1} s^{-1})	d (Å)	d/g
Natural IIa	10 × 10^3	100 to 600		10^{15}	500 to 3000	50	
Film (6 μm)	4.0 × 10^3	44		10^8	~50	880	0.088
Film (3 μm)	3.0 × 10^3	28		10^{10}	~43	360	0.018
dc1	1.0 × 10^3	120	50	250	0.02	0.3	0.002
dc2	4.5 × 10^3	230	Little/no tail	2600	0.12	12	0.006
dc3	4.8 × 10^3	250	Little/no tail	5500	0.07	9	0.002
dc4	3.8 × 10^3	170	20	300	0.02	1.4	0.0002
dc5	4.0 × 10^3	160	Little/no tail	1000	0.16	10	0.0002
dc6	160	550	20	100	3	30	0.020
dc7	150	200	9	100	2	14	0.007
dc8	260	400	None	100	0.2	2	0.001
					±Factor 2		

1.0, with the best value being less than 0.1. If carriers were being trapped out at the grain boundaries, shorter decay times at higher fields would be expected, but this was not observed. Rather, the decay times were independent of the field in all samples.

Although both types of films appear to contain a high density of traps, their nature and energy distribution appear to be different, on the basis of the shape of the decays. The slow tail in the dc films is likely due to carrier detrapping, which involves the capture of electrons (or holes) by a shallow trap level. Thermal excitation then brings these carriers back into the conduction (or valence) band. In the samples with little or no tail, the trap levels may be deep enough that detrapping becomes insignificant. It is possible that just small changes in growth parameters between films is enough to alter the depths and distributions of the traps. It is common in polycrystalline materials to find large densities of traps, either discrete or continuous in energy distribution. An exponential distribution of traps in microwave diamond films has been observed (*12*), and others have reported high densities of acceptor states distributed over several electron volts above the valence band (*28, 29*). In natural single-crystal diamonds, nitrogen impurities play an important role in carrier recombination (*24*). In the case of the polycrystalline diamond films, high densities of defects, most notably dislocations, stacking faults, twins (*30, 31*), and impurities, have been observed, which can act as trapping and recombination sites. In future investigations it will be necessary to relate these structural defects and their densities with measured electrical properties.

Although the electrical properties of polycrystalline diamond are steadily improving, the material is still much poorer in quality than single-crystal natural diamonds. For example, the low-density mobility of the best films studied here is between 10 to 100 times less than that of single-crystal natural diamond. In order to use CVD diamond for device applications, the defect densities must be lowered to improve both lifetime and mobility. The material is promising, however, because of the ability to control the processing. Recent improvements in the quality of the films are encouraging. Epitaxial diamond films have been deposited with properties very close to those of the diamond substrate (*32*), demonstrating that the CVD technique is capable of producing high-quality diamond.

REFERENCES AND NOTES

1. R. Berman, in *Properties of Diamond*, J. E. Field, Ed. (Academic Press, San Diego, CA, 1979), pp. 3–22.
2. J. E. Field, Ed., *ibid.*
3. C. Canali *et al.*, *Nucl. Instrum. Methods* **160**, 73 (1979).
4. G. A. Baraff, *Phys. Rev. A* **133**, 26 (1964).
5. J. Fontanella, R. L. Johnston, J. H. Colwell, C. Andeen, *Appl. Opt.* **16**, 2949 (1977).
6. W. B. Wilson, *Phys. Rev.* **127**, 1549 (1962).
7. R. W. Keyes, *Proc. IEEE* **60**, 225 (1972).
8. A. Johnson, *RCA Rev.* **26**, 163 (1965).
9. G. S. Gildenblat, S. A. Grot, A. Badzian, *Proc. IEEE* **79**, 647 (1991).
10. W. A. Yarbrough and R. Messier, *Science* **247**, 688 (1990); W. Zhu, B. R. Stoner, B. E. Williams, J. T. Glass, *Proc. IEEE* **79**, 621 (1991).
11. M. I. Landstrass and K. V. Ravi, *Appl. Phys. Lett.* **55**, 975 (1989).
12. S. Ashok, K. Srikanth, A. Badzian, T. Badzian, R. Messier, *ibid.* **50**, 763 (1987).
13. Doping, particularly *p*-type, has been achieved with some success, but dopants tend to form deep levels, requiring high concentrations of dopants that can severely limit the carrier mobility.
14. D. R. Kania *et al.*, *J. Appl. Phys.* **68**, 124 (1990).
15. L. S. Pan, P. Pianetta, D. R. Kania, O. L. Landen, K. V. Ravi, in *OSA Proceedings on Picosecond Electronics and Optoelectronics*, T. C. L. G. Sollner and D. M. Bloom, Eds. (Optical Society of America, Washington, DC, 1989), pp. 170–174; L. S. Pan *et al.*, *Electrochem. Soc. Proc.* **89-12**, 424 (1989).
16. E. L. Palik, Ed., *Handbook of Optical Constants of Solids* (Academic Press, Orlando, FL, 1985), pp. 665–673.
17. D. S. Knight and W. B. White, *J. Mater. Res.* **4**, 385 (1989).
18. J. W. Ager III, D. K. Veirs, G. M. Rosenblatt, *Phys. Rev. B* **43**, 6491 (1991).
19. O. L. Landen, M. D. Perry, E. M. Campbell, *Phys. Rev. Lett.* **60**, 1270 (1988).
20. P. S. Panchhi and H. M. van Driel, *IEEE J. Quantum Electron.* **QE-22**, 101 (1986).
21. L. S. Pan, D. R. Kania, P. Pianetta, S. Han, O. L. Landen, in preparation.
22. A. G. Redfield, *Phys. Rev.* **94**, 526 (1954).
23. E. A. Konorova and S. A. Shevchencko, *Sov. Phys. Semicond.* **1**, 299 (1967).
24. L. S. Pan, D. R. Kania, P. Pianetta, O. L. Landen, *Appl. Phys. Lett.* **57**, 623 (1990).
25. K. Okano, personal communication.
26. K. Okano *et al.*, in *New Diamond Science and Technology*, R. Messier, J. T. Glass, J. E. Butler, R. Roy, Eds. (Materials Research Society, Pittsburgh, 1990), pp. 917–924.
27. K. Nishimura, personal communication.
28. K. Okumura, J. Mort, M. Machonkin, *Appl. Phys. Lett.* **57**, 1907 (1990).
29. J. Mort, M. A. Machonkin, K. Okumura, *ibid.* **59**, 455 (1991).
30. B. E. Williams and J. T. Glass, *J. Mater. Res.* **4**, 373 (1989).
31. J. L. Kaae, P. K. Gantzel, J. Chin, W. P. West, *ibid.* **5**, 1480 (1990).
32. L. S. Pan *et al.*, in preparation.

33. This work was performed under the auspices of the U.S. Department of Energy by Lawrence Livermore National Laboratories under contract W-7405-ENG-48 and was also supported by the Stanford Synchrotron Radiation Laboratory, which is supported by the U.S. Department of Energy, Office of Basic Energy Science, Division of Chemical Sciences. In this research P.P. was supported by that office's Division of Material Science. M.L. was supported by the U.S. Air Force at Eglin Air Force Base. The work at Lawrence Berkeley Laboratories was supported by the Director, Office of Energy Research, U.S. Department of Energy, under contract DE-AC-03-76SF00098.

30 September 1991; accepted 6 December 1991

Compressibility of M_3C_{60} Fullerene Superconductors: Relation Between T_c and Lattice Parameter

Otto Zhou, Gavin B. M. Vaughan, Qing Zhu, John E. Fischer,* Paul A. Heiney, Nicole Coustel, John P. McCauley, Jr., Amos B. Smith III

X-ray diffraction and diamond anvil techniques were used to measure the isothermal compressibility of K_3C_{60} and Rb_3C_{60}, the superconducting, binary alkali-metal intercalation compounds of solid buckminsterfullerene. These results, combined with the pressure dependence of the superconducting onset temperature T_c measured by other groups, establish a universal first-order relation between T_c and the lattice parameter *a* over a broad range, between 13.9 and 14.5 angstroms. A small second-order intercalate-specific effect was observed that appears to rule out the participation of intercalate-fullerene optic modes in the pairing interaction.

A number of isostructural binary and pseudobinary alkali metal–C_{60} superconductors have been discovered that have onset temperatures T_c ranging from 18 to 33 K (*1*). Their general formulas are $M_{3-x}M'_xC_{60}$, and their face-centered-cubic lattice parameters *a* range from 14.25 to 14.49 Å at atmospheric pressure and 300 K. A monotonic increase of T_c with alkali size is inferred from an empirical linear correlation between T_c and *a* at constant pressure (*1*). Moreover, T_c decreases with increasing pressure for the binary compounds with M = K (*2, 3*) and Rb (*4*), and the two sets of $T_c(P)$ data can be superposed by a relative shift of the pressure scales (*4*). These results both suggest that T_c depends only on the overlap between near-neighbor C_{60} molecules and not explicitly on the

O. Zhou, Q. Zhu, J. E. Fischer, N. Coustel, Laboratory for Research on the Structure of Matter and Department of Materials Science and Engineering, University of Pennsylvania, Philadelphia, PA 19104.
G. B. M. Vaughan and P. A. Heiney, Laboratory for Research on the Structure of Matter and Department of Physics, University of Pennsylvania, Philadelphia, PA 19104.
J. P. McCauley, Jr., and A. B. Smith III, Laboratory for Research on the Structure of Matter and Department of Chemistry, University of Pennsylvania, Philadelphia, PA 19104.

*To whom correspondence should be addressed.